The F-actin cortical network is a major factor influencing the organization of the secretory machinery in chromaffin cells

Cristina J. Torregrosa-Hetland[1], José Villanueva[1], Daniel Giner[1], Inmaculada Lopez-Font[1], Angel Nadal[2], Iván Quesada[2], Salvador Viniegra[1], Giovanna Expósito-Romero[1], Amparo Gil[3], Virginia Gonzalez-Velez[4], Javier Segura[5] and Luis M. Gutiérrez[1,*]

[1]Instituto de Neurociencias, Centro Mixto Universidad Miguel Hernández-CSIC, Sant Joan d'Alacant, Alicante 03550, Spain
[2]Instituto de Bioingeniería and CIBERDEM Universidad Miguel Hernández, Elche 03202, Spain
[3]Departamento de Matemática Aplicada y Ciencias de la Computación, Universidad de Cantabria, Avd. Los Castros, 39005 Santander, Spain
[4]Área de Química Aplicada, Universidad Autónoma Metropolitana-Azcapotzalco, Av. San Pablo 180, CP 02200, México D.F., México
[5]Departamento de Matemáticas, Estadística y Computación, Universidad de Cantabria, Avd. Los Castros, 39005 Santander, Spain
*Author for correspondence (luisguti@umh.es)

Accepted 26 October 2010
Journal of Cell Science 124, 727-734

doi:10.1242/jcs.078600

Summary

We have studied how the F-actin cytoskeleton is involved in establishing the heterogeneous intracellular Ca^{2+} levels ($[Ca^{2+}]_i$) and in the organization of the exocytotic machinery in cultured bovine chromaffin cells. Simultaneous confocal visualization of $[Ca^{2+}]_i$ and transmitted light studies of the cytoskeleton showed that, following cell stimulation, the maximal signal from the Ca^{2+}-sensitive fluorescent dye Fluo-3 was in the empty cytosolic spaces left by cytoskeletal cages. This was mostly due to the accumulation of the dye in spaces devoid of cytoskeletal components, as shown by the use of alternative Ca^{2+}-insensitive fluorescent cytosolic markers. In addition to affecting the distribution of such compounds in the cytosol, the cytoskeleton influenced the location of L- and P-Q-type Ca^{2+} channel clusters, which were associated with the borders of cytoskeletal cages in resting and stimulated cells. Indeed, syntaxin-1 and synaptotagmin-1, which are components of the secretory machinery, were present in the same location. Furthermore, granule exocytosis took place at these sites, indicating that the organization of the F-actin cytoskeletal cortex shapes the preferential sites for secretion by associating the secretory machinery with preferential sites for Ca^{2+} entry. The influence of this cortical organization on the propagation of $[Ca^{2+}]_i$ can be modelled, illustrating how it serves to define rapid exocytosis.

Key words: Chromaffin cell, Exocytosis, F-actin cytoskeleton, Intracellular Ca^{2+}, SNARE protein, Fluorescence microscopy

Introduction

The function of the F-actin cortex in secretion remains controversial, particularly because it has been assigned various roles, such as being a barrier, being involved in transportation or even being a scaffold in neuronal and neuroendocrine cells (Sankaranarayanan et al., 2003; Trifaro et al., 2008). The concept of the cortical barrier was first established on the basis of the intense peripheral phalloidin staining that appeared to become fragmented during secretion in chromaffin cells (Aunis and Bader, 1988; Trifaro et al., 1992). Since these early studies, our comprehension of the cortical cytoskeleton has evolved as techniques have been introduced that allow the dynamic changes in F-actin during exocytosis to be studied. On the basis of the difference in the interference pattern of transmitted light from an F-actin gel and G-actin in the sol (liquid) state, it has been shown that the cortical cytoskeleton is a dense network of polygonal structures that undergoes dynamic transformations during the secretory process (Giner et al., 2005; Giner et al., 2007). Indeed, these structures extend into the interior of the cell, forming a less dense multipolygonal network. Among the changes observed, Ca^{2+}-dependent transitory disruption of cortical F-actin appears to be associated with the access of vesicles to exocytotic sites (Giner et al., 2005), as required for the replenishment of ready-releasable granule pools (Parsons et al., 1995).

It has been demonstrated that 'hotspots' of Ca^{2+} exist and that they are associated with single-vesicle exocytosis (Robinson et al., 1995). This behaviour would contribute to the generation of heterogeneous intracellular Ca^{2+} levels ($[Ca^{2+}]_i$) that favour the preferential reorganization of the cytoskeleton in specific cortical regions. At such sites, Ca^{2+}-dependent F-actin-cleaving proteins, such as scinderin (Dumitrescu et al., 2005), along with Ca^{2+}-dependent molecular motors, such as myosin II (Neco et al., 2004), might drive the appropriate dynamic transformations, giving vesicle access and allowing their movement towards active zones.

Bearing in mind the complexity of the cytosolic space, we wondered how such complexity could influence the generation and propagation of the $[Ca^{2+}]_i$ signalling that triggers exocytosis in a neuroendocrine (chromaffin) cell model. We demonstrate that the secretory machinery and voltage-dependent Ca^{2+} channels (VDCCs) are located at the borders of cortical cytoskeletal structures. Such an arrangement of the proteins that participate in exocytosis with cytoskeletal cortical cages facilitates local and rapid secretory responses, as witnessed by the direct observation of exocytotic fusion and through the modelling of secretory zone geometry.

Journal of Cell Science

Results

Fluo-3 signals are heterogeneous in the cytosol of cultured chromaffin cells

Ca^{2+} signalling is essential to initiate the secretory process in chromaffin cells. Indeed, cells incubated with Fluo-3 AM and stimulated by fast superfusion of a buffer containing KCl (59 mM) displayed very robust fluorescent signals during the depolarizing pulse (Fig. 1). The nature of this signal was heterogeneous as the rise in the fluorescence signal was not the same in different zones of the cytoplasm. This was especially evident during maximal enhancement of the signal (Fig. 1B), but it was also observed under resting conditions (Fig. 1A) and at the offset of the depolarizing pulse (Fig. 1C). Overall, there was a variable spatial response behind the fivefold enhancement in fluorescence, when normalized to the basal levels (ΔF/Fo; Fig. 1D), which was observed in a number of experiments with different secretagogues.

We examined the factors that might contribute to such spatial variability in the Fluo-3_i response, such as the presence of a complex cytoskeletal network. We studied this possibility as this network can be analysed readily by transmitted light imaging (Giner et al., 2005; Giner et al., 2007); when using this technology, the F-actin cytoskeleton appears as an intricate network formed by polygonal cages that present a dynamic behaviour (Giner et al., 2005). We studied the maximal levels of the Fluo-3 signal in relation to this network during cell stimulation (Fig. 1E; F-actin structures are shown in red, with the maximal Fluo-3 fluorescence levels in green, to better appreciate their spatial coincidence). As can be clearly observed in this representative image, higher levels of Fluo-3 signals were found in the dark cytosolic spaces left in the interior of the cytoskeletal cages. By contrast, in the areas where the cytoskeletal structure was denser, such as at the peripheral cortical barrier, the increases in fluorescence upon stimulation were less evident. A quantitative analysis indicated that the fluorescence intensity in the areas with a dense cytoskeleton was lower than in the areas devoid of cytoskeletal elements (Fig. 1F).

Fluorescent dyes accumulate in the areas devoid of cytoskeletal structures

It is possible that the increase in fluorescence reflected an accumulation of the Ca^{2+} indicators rather than a true enhancement of $[Ca^{2+}]_i$ in the empty spaces left by cytoskeletal structures. We tried to address this issue by performing experiments with ratiometric dyes, such as Fura-2 and Indo-1, but we found that there was too much noise associated with their signals to gain information at the level required to study the cytosolic distribution. Thus, as an alternative, we used additional Ca^{2+}-insensitive fluorescent dyes to normalize the Fluo-3 signals (see Fig. 2 for an example of the use of BODIPY 505/515). The Ca^{2+}-insensitive fluorescent dye BODIPY 505/515, which has a molecular mass that is very similar to that of Fluo-3, was also heterogeneously distributed in the cytoplasm of chromaffin cells (Fig. 2B). When these images were analysed in detail, it was clear that the fluorescent intensity tended to be weaker in the areas occupied by dense cytoskeletal structures, whereas the empty spaces were characterized by higher fluorescent intensities (Fig. 2C–F). More interestingly, the relationship between the BODIPY 505/515 intensity and the density of cytoskeletal structures was linear, demonstrating that the fluorescent dye accumulated preferentially in the empty spaces devoid of cytoskeleton (Fig. 2G). These results were confirmed with other fluorescent dyes, such as the CellTracker Orange CMRA dye, which emits red fluorescence and was used to normalize the intensity of the Fluo-3 signal in cells incubated with both CMRA and Fluo-3 (Fig. 3). A detailed analysis of the normalized fluorescence signal (Fluo-3 fluorescence over the CMRA fluorescence; Fig. 3) indicated that there were no significant changes between the areas with a dense cytoskeleton (Fig. 3, high) and areas with a low density of cytoskeleton (Fig. 3, low), a conclusion validated when the cells were stimulated by depolarization (Fig. 3G) or by incubation with ionomycin in basal medium containing 2 mM Ca^{2+} (Fig. 3H). Taking these data into account, it is clear that the preferential accumulation of fluorescent dyes in the areas (dark spaces) devoid of cytoskeletal structures is a major factor contributing to the heterogeneity of Fluo-3 signals, whereas intracellular Ca^{2+} levels appear to be unrelated to the cytoskeletal structures.

Ca^{2+} channels form clusters associated with the borders of cytoskeletal cages

In order to study another molecular factor related to secretory behaviour that could be affected by the cytoskeletal organization, we visualized both voltage-dependent Ca^{2+} channels (VDCCs) and cortical F-actin by immunocytochemistry, as described previously (Gil et al., 2001; Lopez et al., 2007). As these experiments required fixed and permeabilized cells, F-actin was visualized through

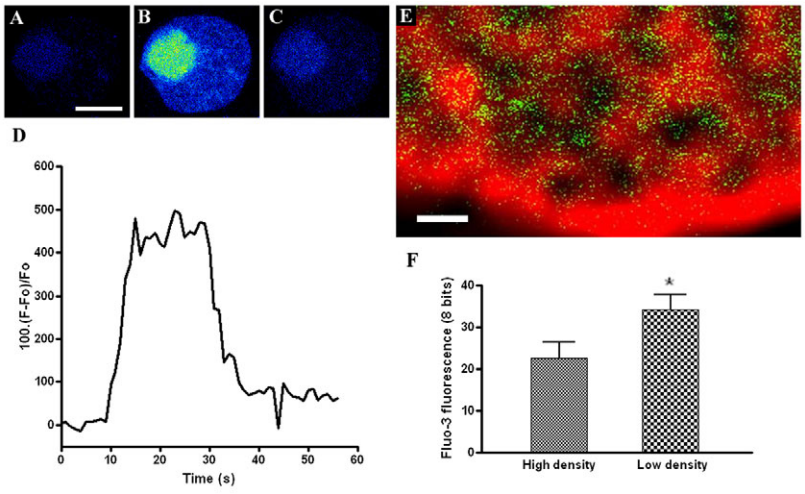

Fig. 1. Heterogeneity of the intracellular Ca^{2+} signal during chromaffin cell stimulation. (**A–C**) Images (16-pseudocolour) of a cell showing resting (A), maximal (B; 2 seconds after cell depolarization with a 59 mM KCl K-H solution) and sustained Fluo-3 fluorescence levels (C; 20 seconds after the end of the KCl pulse). In the three images, spatial heterogeneity of the Fluo-3 signal can be observed, which is integrated (normalized) in (**D**). (**E**) Simultaneous observation of the maximal Fluo-3 signal (in green) and transmitted light images of the F-actin cytoskeleton (red) showing the spatial coincidence of the Fluo-3 hotspots and empty spaces (devoid of the cytoskeleton; dark areas). This image is representative of experiments performed on 43 cells from three different cultures. (**F**) Quantitative analysis of the Fluo-3 signals. The Fluo-3 signals from 18 regions of interest from three different cells were averaged for regions presenting dense cytoskeleton (high density) and dark areas (low density). *P<0.05 in comparison with the regions of dense cytoskeleton (Student's t-test). Error bars represent s.e.m. Scale bars: 10 μm (A); 1 μm (E).

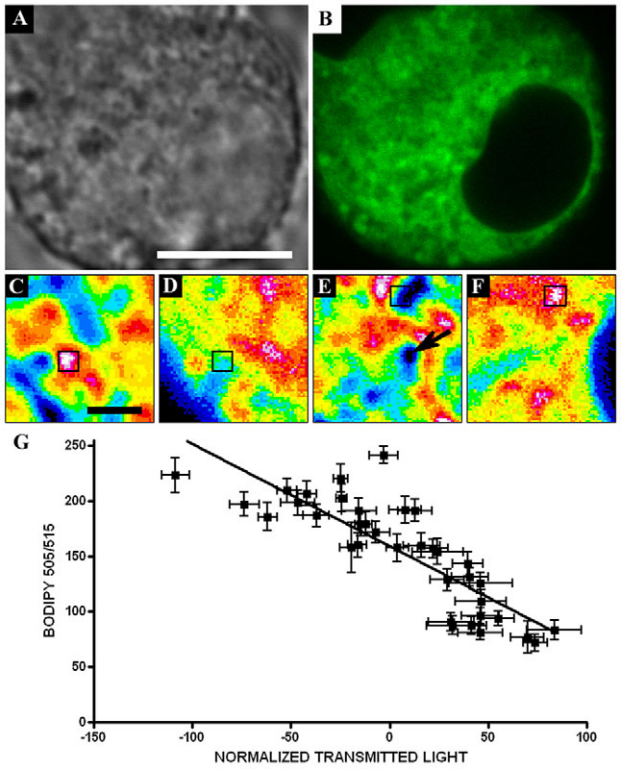

Fig. 2. The fluorescent dye BODIPY 505/515 accumulates in the cytosolic spaces devoid of cytoskeleton in chromaffin cells. Chromaffin cells were incubated with the fluorescent dye BODIPY 505/515 as described in the Materials and Methods section, and the transmitted light (**A**) and fluorescent signal (**B**) were acquired at 1-second intervals on a confocal microscope. (**C**) and (**E**) show pseudocolour images of cytoskeletal structures with different transmitted light intensities; (**D**) and (**F**) depict the BODIPY 505/515 fluorescence intensity in the same cytosolic regions. The regions of interest (ROIs) indicated are representative of the regions selected to compare the intensities in both the transmitted light and fluorescent channels. (**G**) The relationship between the intensity of both channels in the ROIs selected from six different cells. The line represents the best fit to a linear model (R^2=0.71), indicating an inverse correlation between both channels. Error bars represent s.e.m. Scale bars: 5 µm in A; 1 µm in C.

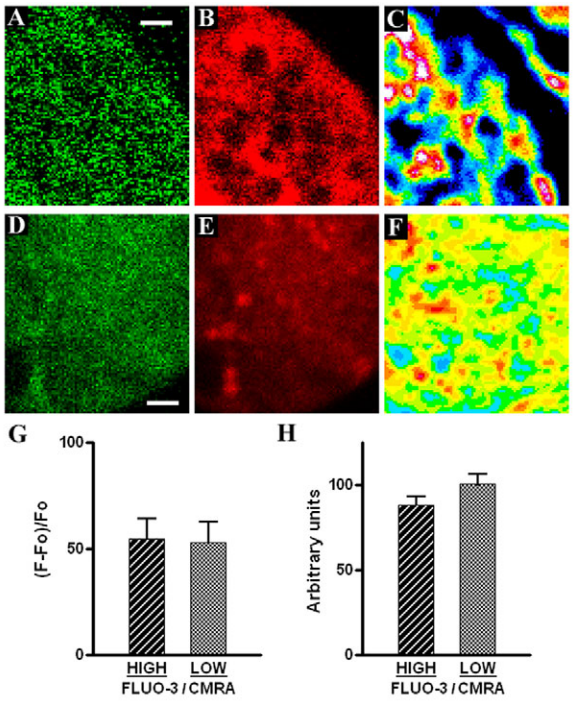

Fig. 3. Normalized Ca^{2+} signals do not differ in distinct areas of the cytosol. Chromaffin cells were labelled with Fluo-3 (**A** and **D**) and the red-fluorescent dye CMRA (**B** and **E**), and the transmitted light was acquired simultaneously in the fluorescent channels (pseudocolour images in **C** and **F**). The cells were then stimulated with 20-second depolarizations in a 59 mM KCl solution (an example experiment is shown in A–C) or by incubation with 5 µM ionomycin (D–F). Ca^{2+} increments were normalized using the ratio of the Fluo-3 signal to the CMRA intensity in the same regions of interest. This ratiometric signal was then averaged for at least eight different regions with either high (dense cytoskeleton) or low (empty cytosolic spaces) transmitted light intensities (**G**,**H**). The results indicate that both KCl depolarization and ionomycin induced an increase in the normalized fluorescent signal. However, this increase was not significantly different when regions with dense cytoskeleton were compared with regions with low transmitted light intensity. Error bars represent s.e.m. Scale bars: 1 µm.

rhodamine–phalloidin staining. In confocal images of cells labelled with either a rabbit polyclonal antiserum against L-type (Hui et al., 1991) or P-Q-type VDCCs (Starr et al., 1991), round clusters of channels were clearly associated with the phalloidin-labelled bundles forming the F-actin network before and after stimulation. Inspection of the images obtained in resting cells revealed that the VDCC clusters were preferentially located at the borders of the heterogeneous open spaces formed by the F-actin cortex (Fig. 4A,C). After stimulation, the average size of the F-actin-vacant areas increased and most of the Ca^{2+} channel clusters appeared at the borders of the F-actin bundles. To support this conclusion at the statistical level, we estimated the number of clusters colocalizing, at least partially, with F-actin labelling and those colocalizing with dark empty-space pixels, resulting in percentage values of over 90% for the total microdomains for both subtypes of Ca^{2+} channels (Fig. 4E). Furthermore, the estimation of Ca^{2+} channel patches presenting both conditions (i.e. colocalizing with F-actin labelling and with dark empty-space pixels), thus locating in the borders, was also over 90% for both types of Ca^{2+} channels; these values clearly differ from the percentage estimated for randomly located microdomains of similar size (65%). We also confirmed these results by analysing the distance between VDCC microdomains and F-actin labelling; the average distance was significantly lower for real patches compared with that for the randomly generated domains (Fig. 4F). This was also evident when observing the distance distributions for the three types of microdomains – the percentage of patches located at a distance greater than 200 nm increases from 3% for the real VDCC domains to 34% for the randomly generated domains (Fig. 4G). Taken together, we conclude that L- and P-Q-type VDCC microdomains locate at the borders of F-actin structures, suggesting a functional relevance for specific areas of the cortical network.

The secretory machinery is associated with the borders of the cortical F-actin cages

The location of VDCCs at the borders of the cytoskeletal structures suggests that these areas could participate in defining the active sites for exocytosis. We tested this hypothesis by studying the distribution of the SNARE proteins, which form

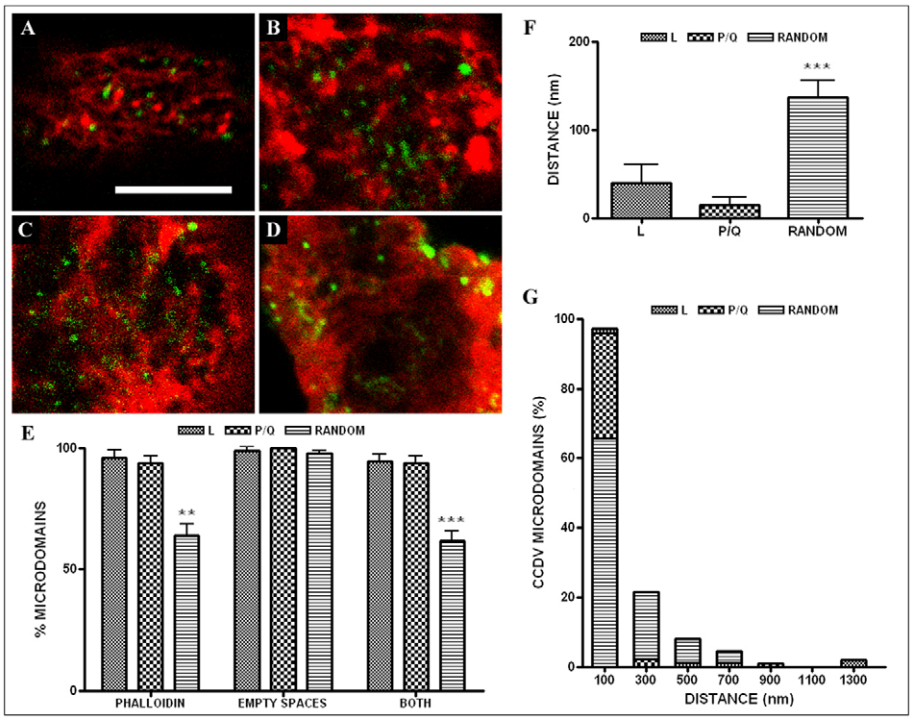

Fig. 4. P-Q- and L-type VDCCs are associated with the borders of F-actin structures. Chromaffin cells were depolarized in 59 mM KCl for 5 minutes and they were then fixed and permeabilized as described in the Materials and Methods section. Primary rabbit polyclonal antisera against P-Q-type (**A**,**B**) or L-type (**C**,**D**) VSCCs were used to visualize the location of clusters by confocal microscopy of cortical areas in control unstimulated cells (A and C) and in depolarized cells (B and D). After incubation with secondary antibodies coupled to FITC (green fluorescence), F-actin was labelled using rhodamine–phalloidin (red fluorescence). Scale bar: 5 µm. (**E**) An analysis of the colocalization of the clusters of Ca^{2+} channels with either phalloidin labelling (sharing pixels with 50% of the maximal intensity in the two channels), with empty spaces or where both conditions were fulfilled (clusters located at the borders of F-actin). As an additional control, the colocalization of L-type (97 clusters from four cells) and P-Q VDCC clusters (105 clusters from four cells) were compared with that in randomly generated clusters (392 clusters in 14 images). The results indicated that both L- and P-Q-type VDCC microdomains present a high probability (>92%) of sharing pixels with phalloidin labelling, whereas randomly generated clusters present a lower probability (<65%). The vast majority of the VDCC clusters are associated with the phalloidin-labelled F-actin border. (**F**,**G**) Averaged distance (F) and distributions (G) measured between the L- and P-Q-type VDCC microdomains and the border of cytoskeletal F-actin structures. Results obtained with the randomly generated patches are also shown. Error bars represent s.e.m. $^{**}P<0.01$ and $^{***}P<0.001$ when compared with the percentage obtained with VDCC microdomains.

part of the secretory machinery. These experiments were performed using a chicken antibody against syntaxin-1, which has been previously shown to label SNARE microdomains in our cultured cells (Lopez et al., 2007), and rhodamine–phalloidin. Syntaxin-1 labelling was clearly associated with the margins of the F-actin cytoskeletal cages labelled with phalloidin (Fig. 5). Moreover, upon stimulation, the labelling of the SNARE proteins always appeared to be in contact with the borders of the cytoskeleton and not localized in the centre of the open spaces generated by F-actin reorganization. Thus, the appropriate localization of the secretory machinery and VDCC clusters to the borders of the F-actin cages that form a cortical network in chromaffin cells influences the location of the secretory response to the areas where preferential reorganization of the F-actin network might ensure a supply of new vesicles. This hypothesis was tested further by performing triple-labelling experiments with an antibody against synaptotagmin-1, which is a Ca^{2+}-sensor protein associated with the SNARE core complex, as well as with an antibody against P-Q-type VDCCs and with phalloidin coupled to CPITC. Synaptotagmin-1 (Fig. 5C) and the Ca^{2+} channel clusters (Fig. 5D) clearly colocalized, and they appeared to contact the borders of the spaces devoid of F-actin (Fig. 5F). Thus, it appears that the secretory machinery colocalized with the VDCC domains and, therefore, with the borders of cytoskeletal cages. It also appears that, for a given SNARE cluster, multiple VDCC clusters (usually between two and three according to the images obtained in 18 cells from two cultures) will ensure the Ca^{2+} elevations needed for triggering exocytosis.

Granule fusion occurs in areas in contact with the walls of cytoskeletal cages

Given that the elements constituting the secretory machinery associate with the borders of the cytoskeletal cages, granules might interact with cytoskeletal elements even at the time of exocytosis. To determine whether this interaction occurs, we studied the precise site of exocytosis by examining the exocytotic events in vivo using total internal reflection fluorescence microscopy (TIRFM) observation of granules from cells expressing GFP–synaptobrevin-II and compared the location with that of the cytoskeletal structures visualized by transmitted light. GFP-labelled vesicles appeared to interact with the borders of cytoskeletal cages, avoiding the empty spaces left in the interior of such structures (Fig. 6; supplementary material Movie 1). This interaction continued until the moment of vesicle fusion, when the KCl depolarizing solution superfused the cells. However, we observed no vesicle fusion in areas devoid of cytoskeletal structures (284 fusions from 23 cells).

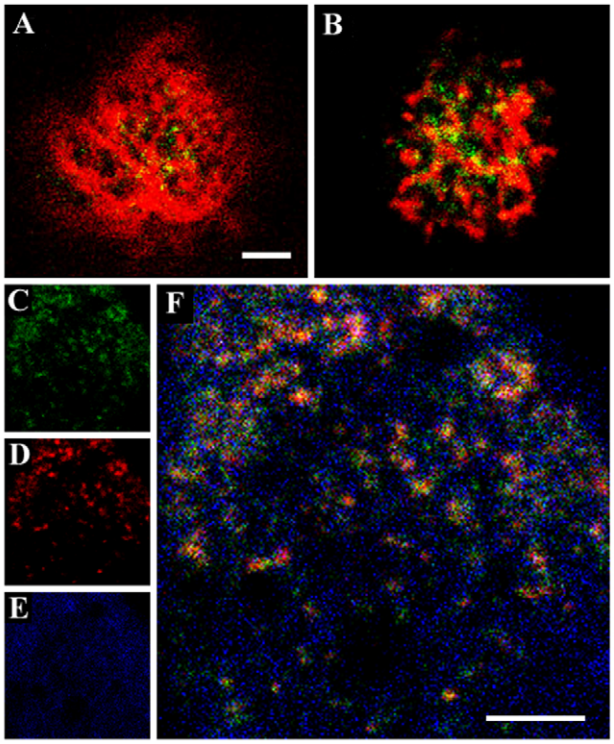

Fig. 5. Clusters of syntaxin-1 and synaptotagmin-1 are associated with the borders of F-actin domains and VDCC microdomains. The components of the secretory machine were labelled using anti-syntaxin-1 or anti-synaptotagmin-1 antibodies raised in chicken. (**A**,**B**) Confocal images of polar sections of control (A) and depolarized cells (B) showing the distribution of syntaxin labelling (green) and F-actin-bound rhodamine–phalloidin (red). (**C**–**F**) Similar confocal images depicting triple-labelling experiments with antibodies against synaptagmin-1 (green, C) and P-Q-type VDCC (red, D), as well as phalloidin coupled to CPITC (blue, E) in stimulated cells. F shows the overlay of the three labels. Scale bars: 2 μm.

In addition, we performed experiments using antibodies against dopamine β-hydroxylase, to detect incorporation of vesicle membrane into the plasmalemma after exocytosis, in combination with F-actin labelling with rhodamine–phalloidin. These in vitro experiments confirmed the observations in live cells, and even in the occasional fusion events observed in unstimulated cells, secretory spots labelled with antibodies against dopamine β-hydroxylase were seen adjacent to the borders of fluorescently labelled cytoskeletal cages (data not shown). Taken together, these two approximations strongly suggest that the fusion of the vesicles occurs at the border of the cortical cytoskeletal structures as predicted by the distribution of the secretory machinery elements and VDCCs.

Discussion

The results obtained in the present study lead us to conclude that the association of the secretory machinery and the clusters of VDCCs with the borders of cortical cytoskeletal cages determines the precise site for exocytosis in chromaffin cells. In addition, this specific cytoarchitecture might contribute to the secretory kinetics and limit the cytoplasmic diffusion of relatively small molecules, such as Ca^{2+} indicators.

Cytoskeletal organization and the distribution of fluorescent Ca^{2+} indicators

Heterogeneity in $[Ca^{2+}]_i$ signalling has been described as a characteristic feature of intracellular signalling in chromaffin cells (O'Sullivan et al., 1989). It has been suggested that the possible cause of such heterogeneity is through the Ca^{2+} hotspots that are generated in the membrane (Monck et al., 1994) or even through Ca^{2+} release from intracellular reservoirs, such as mitochondria (Pozzan and Rizzuto, 2000; Montero et al., 2002) or the endoplasmic reticulum (ER) (Burgoyne et al., 1989). One simple explanation for this heterogeneity is the organization of the cytosolic space itself, which is structured as a dense intricate network of dynamic cytoskeletal polygonal cages that can be readily studied in live cells by transmitted-light microscopy (Giner et al., 2005; Giner et al., 2007). Our relatively simple experimental approach enabled us to demonstrate that the F-actin cytoskeleton must be taken into consideration in order to understand the heterogeneity in Fluo-3 signals. It is probable that the condensed gel state of F-actin does not allow the free diffusion of Ca^{2+} indicators, thereby influencing $[Ca^{2+}]_i$ measurements, which have to be corrected for dye heterogeneity. However, these results do not mean that relatively small molecules cannot spread through the cytoplasm as the cytoskeletal cages are interconnected (Giner et al., 2005).

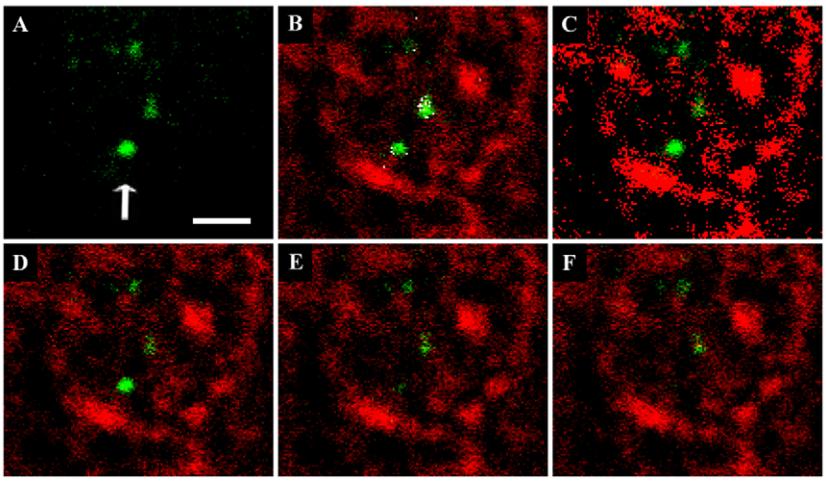

Fig. 6. Vesicles in contact with the walls of cytoskeletal cages undergo fusion. Cultured cells expressing GFP–synaptobrevin-II (green) were visualized by TIRFM in combination with transmitted light images (red), and exocytosis was stimulated by KCl depolarization. The arrow indicates the chromaffin granule fusing during the experiment. (**A**) Vesicles that were found to interact with the transmitted light structures (colocalized pixels containing more than 50% of the intensity in both channels, as shown in white in **B**). (**C**) A depiction of the pixels with more than 50% of the maximal intensity in the transmitted light channel (red), to show the vesicles situated at the border of the cages. (**D**–**F**) A sequence of images, each separated by 1 second, depicting the continuous interaction of the three brightest vesicles with cytoskeletal cages. After depolarization, the largest vesicle fused rapidly (panel E) and, at the time of fusion, it was still in contact with the cytoskeletal structures. Scale bar: 10 μm.

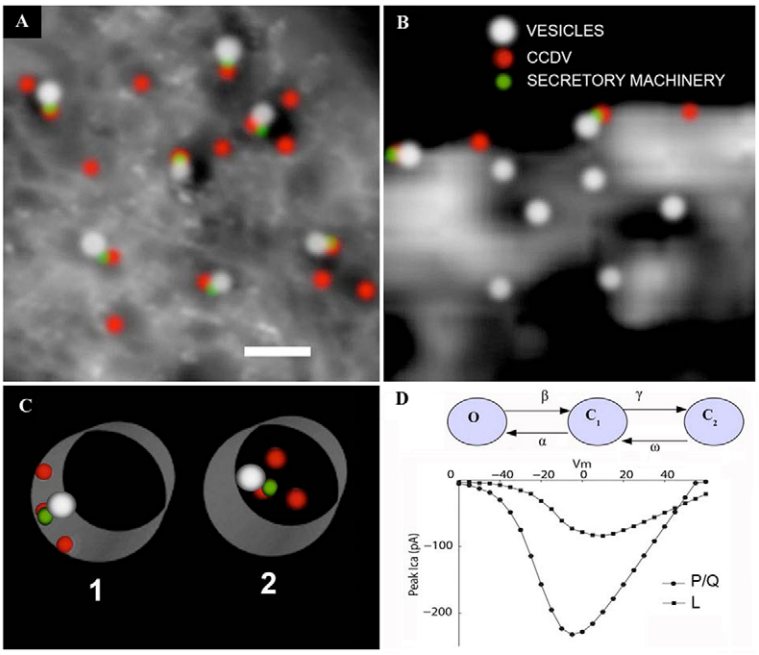

Fig. 7. A model to study the influence of the cytoskeleton in secretion. According to our data, we envisage the cytoskeleton as an intricate network where VDCCs (red circles) and SNARE clusters (green dots) are associated with the borders of cytoskeletal cages, as can be observed from a top polar (**A**) or transverse view (**B**). Vesicles (white circles) could move through the F-actin structures (represented here by real transmitted light images in grey) to reach the docking sites (SNARE microdomains, some of them colocalizing with VDCC clusters). In this model, there are two or three VDCC clusters per SNARE microdomain, fitting our experimental observations. Scale bar: 1 µm. (**C**) Simplified mathematical model. Arrangements of three clusters of Ca^{2+} channels in a cylindrical domain that represents the averaged cytoskeletal cage considered in the simulations. Configuration 1 has the channels located at the border of a cortical F-actin cage. In configuration 2, the clusters of channels are located at the centre of the cage. (**D**) A three-state model and current-to-voltage relationships simulated for P-Q- and L-type Ca^{2+} channels. O represents the open state, C_1 represents the closed state and C_2 represents the inactive state arising from Ca^{2+} inactivation.

Functional consequences of the organization of the secretory machinery in association with cortical cytoskeletal cages in chromaffin cells

We show that the secretory machinery, as visualized here by syntaxin-1 and synaptotagmin-1 immunostaining, clearly associates with the margins of cytoskeletal cortical structures in our cellular model. Furthermore, these proteins also partially colocalize with VDCCs, although the clusters formed by these channels are more abundant and exceed the size of the secretory machinery spots by twofold to threefold. Therefore, we propose a model to explain the organization of the secretory apparatus that is in association with the borders of the cytoskeletal polygonal cages forming the cortical mesh. In this model (Fig. 7), the secretory machinery appears to associate with the borders of the dense F-actin structures, represented here by a three-dimensional reconstruction of a region from a real chromaffin cell. From above the cortex, we observe numerous cages of varied shapes and sizes, with secretory machinery clusters appearing at their border and interacting with some VDCC clusters. In a transverse view of the cortical region (Fig. 7B), these secretory and VDCC clusters are located in the upper zone of the F-actin structure, close to the plasma membrane, where they can tether approaching vesicles. In our model, the

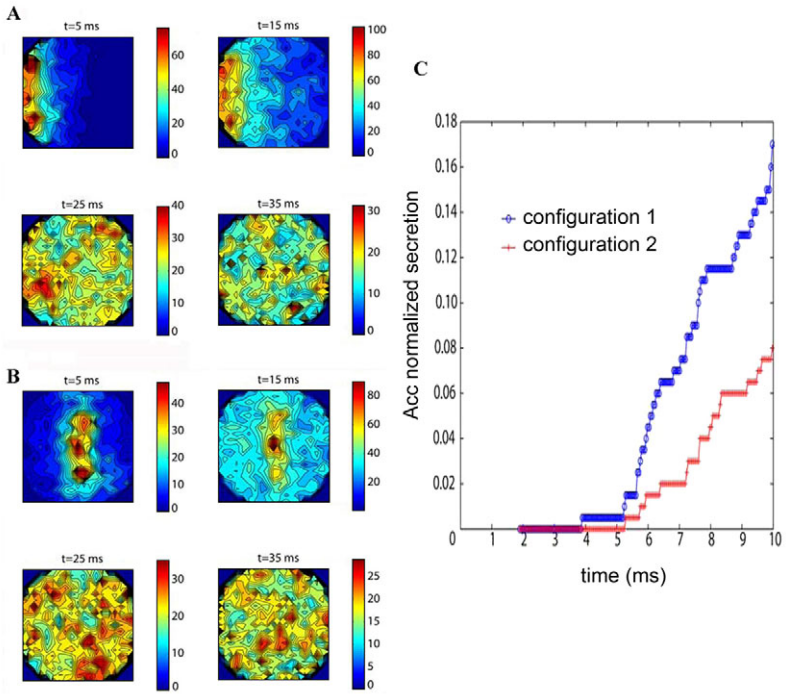

Fig. 8. Modelling the distribution of the secretory machinery elements in the borders of cytoskeleton cages shows an enhancement in the secretory kinetics. Using the model described in Fig. 7, a short depolarizing pulse from –80 to 20 mV that starts at *t*=2 mseconds is simulated. (**A**,**B**) The Ca^{2+} maps for configurations 1 and 2 (A and B, respectively) obtained for a submembrane region between 0 and 30 nm from the cell membrane at *t*=5, 15, 25 and 35 mseconds. (**C**) Secretory response kinetics. The secretory response for the short voltage pulse was also simulated and the normalized accumulated secretory response plotted during the first 10 mseconds for both configurations.

vesicles will 'encounter' the exocytotic sites travelling through the F-actin surface structure, as observed previously (Giner et al., 2005). A consequence of the proposed model is that, in the proximity of a granule docked to the secretory cluster, the $[Ca^{2+}]_i$ could be increased through the associated VDCC cluster, as well as through other VDCC clusters located at the borders of the same cytoskeletal cage, and, therefore, in the vicinity of this granule. The occurrence of several VDCC clusters in a cytoskeletal cage will have an additive effect on the $[Ca^{2+}]_i$ levels reached in the interior of cytoskeletal cages.

A model to understand the functional implications of the existence of an F-actin polygonal network in the cortical region of secretory cells

To evaluate the benefits of having such an intricate network of F-actin near the active sites of exocytosis, we have conceived a simple geometric model of the secretory zone (Fig. 7C). We have modelled cytoskeletal cages as cylindrical domains of 0.6 μm diameter [the average size of cortical cages (Giner et al., 2007)], where three VDCC clusters and an active secretory site are located either at the walls ('configuration 1') or at the centre ('configuration 2') of this structure. A Monte Carlo algorithm was used to simulate the stochastic processes, taking in account the Ca^{2+} influx through L- and P-Q-type VDCCs (the channel properties are modelled in Fig. 7D), as well as the endogenous buffering and kinetics of vesicle fusion [according to the parameters defined by Segura and colleagues (Segura et al., 2000); see table 1 within]. Quantification of the two geometries, to determine which led to faster secretion, resulted in $[Ca^{2+}]_i$ maps with submembrane domains of up to 30 nm in diameter in response to short depolarizations to –20 mV (from a resting potential of –80 mV) (Fig. 8A,B). These maps show that configuration 1 resulted in the most robust initial rise in $[Ca^{2+}]_i$ in the proximity of the active site (see the panels at 5 and 15 mseconds after initiating the response), whereas over prolonged periods the $[Ca^{2+}]_i$ homogenizes for both configurations. Interestingly, the simulated $[Ca^{2+}]_i$ maps show a faster exocytotic response when the active site and Ca^{2+} channels form clusters associated with the border of a cytoskeletal cage (Fig. 8C). The results of our simulations indicate that this 'wall effect' is mostly due to the coincidence of higher local Ca^{2+} elevations in the proximity of the cytoskeletal border where the secretory machinery ('the Ca^{2+} sensor') is localized, whereas in the centre of the cage Ca^{2+} levels distribute in a wider volume and local Ca^{2+} elevations dissipate.

In summary, the present study provides us with a provocative new view of how cytoskeletal architecture contributes to the organization of the secretory machinery in neuroendocrine cells, thereby generating an efficient environment that optimizes coupling of the elements constituting the exocytotic machinery and producing faster secretory kinetics.

Materials and Methods

Chromaffin cell preparation, culture and treatment

Chromaffin cells were isolated from bovine adrenal glands by collagenase digestion, and they were separated further from the debris and erythrocytes by centrifugation on Percoll gradients, as described previously (Gutierrez et al., 1997). The cells were maintained as monolayer cultures in Dulbecco's modified Eagle's medium (DMEM) supplemented with 10% foetal calf serum, 10 μM cytosine arabinoside, 10 μM 5-fluoro-2′-deoxyuridine, 50 units/ml penicillin and 50 μg/ml streptomycin. The cells were plated at a density of 80,000 cells per cm^2 on round coverslips and cultured in 35-mm-diameter Petri dishes (Costar). Cells were used between the second and sixth day after plating.

Dynamic study of $[Ca^{2+}]_i$ levels and cytoskeletal structures using confocal microscopy

Cultured cells were incubated for 30 minutes with 2 μM Fluo-3 AM (Molecular Probes), prepared in DMEM using a pluronic dispersing agent, and the cells were then washed three times with K-H (Krebs-HEPES) basal solution comprising: 134 mM NaCl, 4.7 mM KCl, 1.2 mM KH_2PO_4, 1.2 mM $MgCl_2$, 2.5 mM $CaCl_2$, 11 mM glucose and 15 mM HEPES, pH 7.4. The cells were transferred into an Attofluor cell chamber (Molecular Probes) and stimulated with a depolarizing K-H solution containing 59 mM potassium (obtained by isosmotically replacing NaCl with KCl). In some experiments, BODIPY 515/550 (green fluorescence) or CellTracker Orange CMRA (CMRA, red fluorescence) (both from Molecular Probes) were used at 2 μM to investigate the cytosolic distribution of fluorescent dyes and to normalize the Fluo-3 signals. Fluorescence was visualized on an Olympus Fluoview FV300 confocal laser system coupled to an Olympus IX-71 inverted microscope using a 100× PLANAPO oil-immersion objective (1.4 NA) and with an excitation wavelength of 488 nm (argon ion laser, 40 mW; Melles Griot, Carlsbad). This system permits *z*-axis reconstruction, with a theoretical *z*-slice of ~0.5 μm, and sequential mode studies in double-labelling experiments. Transmitted light images were acquired simultaneously using the channel implemented in the confocal microscope, which has been demonstrated previously to be an adequate technique to visualize the organization of the F-actin cytoskeleton in chromaffin cells (Giner et al., 2005; Giner et al., 2007).

Confocal microscopy studies of the cellular distribution of syntaxin-1, synaptotagmin-1 and of Ca^{2+} channel subtypes

Cells were fixed and permeabilized using a modified version (Aunis et al., 1980) of the method described by Lazarides (Lazarides, 1976). Briefly, cells were fixed using 4% paraformaldehyde (PFA) in PBS for 20 minutes. The cells were then permeabilized by a 10-minute incubation with 0.2% Triton X-100 in 3.6% formaldehyde and then washed twice with 1% BSA in PBS over 20 minutes.

Labelling of syntaxin-1A and synaptotagmin-1 (chicken antibodies generously provided by Bazbek Davletov, MRC Laboratory of Molecular Biology, Cambridge, UK) was performed overnight at a 1:200 dilution in PBS. After extensive washing, secondary rabbit anti-(chicken Ig) antibodies coupled to FITC (1:200 dilution; Sigma) were added, and after 2 hours, the unbound material was washed away in PBS. Ca^{2+} channel subtypes were labelled using rabbit polyclonal antisera (Alomone Labs, Jerusalem, Israel), as described previously (Gil et al., 2001; Lopez et al., 2007). The antiserum against the L-type channel was raised against a highly purified peptide corresponding to residues 809–825 of the α1D subunit of rat brain VDCC (Hui et al., 1991), which had been affinity-purified on an immobilized column of the same peptide. The antiserum against the P-Q-type channels was raised against residues 865–881 of the α1A subunit (Starr et al., 1991) of rat brain VDCC. Immunolabelling was performed, as described above, using a 1:200 dilution of the antibodies, and nonspecific labelling was examined using antibody solutions pre-incubated with 3 μg/ml of the corresponding peptides for 1 hour at room temperature. F-actin labelling was performed over 30 minutes using 1 μM rhodamine–phalloidin followed by extensive washing (in some triple-labelling experiments, phalloidin coupled to CPITC was used instead).

Spatial determination of secretion by the immunodetection of the incorporation of dopamine β-hydroxylase into the plasma membrane

Before stimulation of exocytosis, the culture medium was replaced with a basal K-H solution and the cells were stimulated for 5 minutes using a high-potassium (59 mM) depolarizing K-H solution (obtained by isosmotically replacing NaCl with KCl). To prevent vesicle membrane withdrawal by endocytosis, at the end of stimulation the medium was replaced with ice-cold basal K-H solution lacking $CaCl_2$. Cells were incubated with a rabbit antibody against dopamine β-hydroxylase in an ice-cold K-H buffer for 120 minutes (1:500 dilution; Oncogene Research Products, Cambridge, UK), washed and fixed as described above. After extensive washing, a secondary goat anti-(rabbit Ig) antibody coupled to FITC was employed to detect dopamine β-hydroxylase incorporation into the plasmalemma (1:200 dilution; Sigma). Finally, the cells were mounted and their fluorescence examined by confocal microscopy.

Total internal reflection fluorescence microscopy studies of vesicular fusion combined with cortical cytoskeleton visualization by transmitted light in live cells

A through-the-lens TIRFM system was configured in the Olympus IX-71 inverted microscope using a 60× PlanApo 1.45 NA Olympus TIRFM objective. Epifluorescence and laser illumination were selected using an Olympus TIRFM IX2-RFAEVA combiner system, modifying the angle of laser incidence. Fluorescence emission was split using an Optosplit II system (Cairn Research, Faversham, UK) equipped with GFP and rhodamine filter sets. The separated images were simultaneously acquired, side-by-side, at 20 mseconds per frame using an Electron Multiplier CCD cooled camera (C9100-02; Hamamatsu photonics, Japan). TIRFM calibration was performed using 100-nm fluorescent beads (Molecular Probes). The fluorescence intensities were determined at different vertical planes, with step lengths of 100 nm, using the motorized system mounted on the microscope, and the image was obtained for both epifluorescence and TIRFM. The depth of penetration for the

evanescent field was estimated as ~200 nm (1/e depth of 180±16 nm), mainly permitting the visualization of the static beads adhered onto the coverslip. By contrast, beads in suspension undergoing random movement were infrequently seen by the TIRFM and the vast majority were visualized by epifluorescence. Vesicles were visualized using GFP–synaptobrevin-II, as described previously (Gil et al., 2002). In other experiments, vesicles were stained with 2 μM Acridine Orange, and the granule position was assessed by the red Acridine Orange fluorescence of mature acidic vesicles; their fusion was followed by detection of the green flashes produced after matrix neutralization during exocytosis (Lopez et al., 2009). To combine cytoskeletal images with TIRFM, the light from the halogen lamp used for light transmission was filtered to give red light (LP590 filter) for the simultaneous visualization of the labelled vesicles. In that way, the images acquired after separation by the image splitter corresponded to the epifluorescence emission of the lysophilic dye loading the vesicles excited by the evanescence field and the transmitted light image of the cytoskeletal structures.

Modelling the influence of the cytoskeleton in chromaffin cell secretion

A Monte Carlo algorithm was used to simulate, as stochastic processes, the three-dimensional entry of Ca^{2+} ions through L- and P-Q-type channels, Ca^{2+} and mobile buffer diffusion, endogenous buffering of Ca^{2+} and the kinetics for vesicle fusion (Segura et al., 2000). These processes take place in a cylindrical domain representing a prototypic cage in the cortical cytoskeletal network, where channel clusters might locate either at the boundaries (configuration 1) or in the centre of the cage (configuration 2). In bovine chromaffin cells, the total channel population consists of P-Q-, L- and N-type channels [comprising 50%, 20–38% and 12–30%, respectively, of the whole-cell Ca^{2+} current (Garcia et al., 1998; Lukyanetz and Neher, 1999; Garcia et al., 2006)]. As the first two channel types are known to localize preferentially at secretory sites, they can be modelled to simulate exocytosis in bovine chromaffin cells. For modelling purposes, we considered the minimum Ca^{2+} channel population reported for chromaffin cells (five channels per μm^2) (Klingauf and Neher, 1997), which generates about 3500 channels for a cell with a 7.5-μm radius. Thus, representative quantities of the channels chosen to test our simulations were 700 (20%) L-type and 1750 (50%) P-Q-type channels. As the whole-cell conductance of P-Q-type channels has been estimated to be ~4 nS, we defined a unitary conductance of 2.5 pS, which corresponds to at least 1600 channels. For L-type channels, we use a value of 8.4 pS, which corresponds to ~700 channels, giving a whole-cell conductance of 5.9 nS, as estimated for this type of cell (Bossu et al., 1991). L-type channel conductance appears to change as the membrane potential varies; therefore, we fitted smaller values at higher voltages.

The binding and unbinding kinetics of Ca^{2+} ions to binding sites is described by first-order kinetic equations for both the endogenous buffer and the vesicles. All the simulations include the effect of a single immobile endogenous buffer (Klingauf and Neher, 1997). The model was used to simulate Ca^{2+} maps in response to short depolarizations for both configurations and for the submembrane region between 0 and 30 nm. For vesicle fusion, we used a non-cooperative kinetic scheme in which three Ca^{2+} ions have to bind to the Ca^{2+} sensor to access a pre-fusion state. Accordingly, vesicle fusion then occurs following a constant rate of 1 per msecond, which represents the delay between fusion and release (Klingauf and Neher, 1997).

This work was supported by grants from the Spanish Ministry of Education and Culture (MEC, MICINN, BFU2005-02154/BFI and BFU2008-00731) and the Generalitat Valenciana (ACOMP06/036) to L.M.G.; the Spanish Ministry of Education and Culture (BFU2007-67607) and AN (BFU2008-01492) to I.Q.; and the Fundación BBVA and I-MATH project C3-0136 to A.G. and J.S. C.J.T.-H. and I.L.-F. were recipients of fellowships from the MICINN (Spain). V.G-V. thanks CONACyT for its financial support of her PhD scholarship. We also acknowledge the financial support received from the CONSOLIDER programme (CSD07-00023) and CIBERDEM (Instituto de Salud Carlos III).

Supplementary material available online at
http://jcs.biologists.org/cgi/content/full/124/5/727/DC1

References

Aunis, D. and Bader, M. F. (1988). The cytoskeleton as a barrier to exocytosis in secretory cells. *J. Exp. Biol.* **139**, 253-266.

Aunis, D., Guerold, B., Bader, M. F. and Cieselski-Treska, J. (1980). Immunocytochemical and biochemical demonstration of contractile proteins in chromaffin cells in culture. *Neuroscience* **5**, 2261-2277.

Bossu, J. L., De Waard, M. and Feltz, A. (1991). Two types of calcium channels are expressed in adult bovine chromaffin cells. *J. Physiol.* **437**, 621-634.

Burgoyne, R. D., Cheek, T. R., Morgan, A., O'Sullivan, A. J., Moreton, R. B., Berridge, M. J., Mata, A. M., Colyer, J., Lee, A. G. and East, J. M. (1989). Distribution of two distinct Ca2+-ATPase-like proteins and their relationships to the agonist-sensitive calcium store in adrenal chromaffin cells. *Nature* **342**, 72-74.

Dumitrescu, P. T., Rose, S. D., Lejen, T., Marcu, M. G. and Trifaro, J. M. (2005). Expression of various scinderin domains in chromaffin cells indicates that this protein acts as a molecular switch in the control of actin filament dynamics and exocytosis. *J. Neurochem.* **92**, 780-789.

Garcia, A. G., Albillos, A., Cano-Abad, M. F., Garcia-Palomero, E., Hernandez-Guijo, M., Herrero, C. J., Lomax, R. B. and Gandia, L. (1998). Calcium channels for exocytosis in chromaffin cells. *Adv. Pharmacol.* **42**, 91-94.

Garcia, A. G., Garcia-de-Diego, A. M., Gandia, L., Borges, R. and Garcia-Sancho, J. (2006). Calcium signaling and exocytosis in adrenal chromaffin cells. *Physiol. Rev.* **86**, 1093-1131.

Gil, A., Viniegra, S., Neco, P. and Gutierrez, L. M. (2001). Co-localization of vesicles and P/Q Ca2+-channels explains the preferential distribution of exocytotic active zones in neurites emitted by bovine chromaffin cells. *Eur. J. Cell Biol.* **80**, 358-365.

Gil, A., Gutiérrez, L. M., Carrasco-Serrano, M. C., Alonso, T., Viniegra, S. and Criado, M. (2002). Modifications in the C-terminus of the synaptosome-associated protein of 25 kDa (SNAP-25) and in the complementary region of synaptobrevin affect the final steps of exocytosis. *J. Biol. Chem.* **277**, 9904-9910.

Giner, D., Neco, P., Frances, M. M., Lopez, I., Viniegra, S. and Gutierrez, L. M. (2005). Real-time dynamics of the F-actin cytoskeleton during secretion from chromaffin cells. *J. Cell Sci.* **118**, 2871-2880.

Giner, D., Lopez, I., Villanueva, J., Torres, V., Viniegra, S. and Gutierrez, L. M. (2007). Vesicle movements are governed by the size and dynamics of F-actin cytoskeletal structures in bovine chromaffin cells. *Neuroscience* **146**, 659-669.

Gutierrez, L. M., Viniegra, S., Rueda, J., Ferrer-Montiel, A. V., Canaves, J. M. and Montal, M. (1997). A peptide that mimics the C-terminal sequence of SNAP-25 inhibits secretory vesicle docking in chromaffin cells. *J. Biol. Chem.* **272**, 2634-2639.

Hui, A., Ellinor, P. T., Krizanova, O., Wang, J. J., Diebold, R. J. and Schwartz, A. (1991). Molecular cloning of multiple subtypes of a novel rat brain isoform of the alpha 1 subunit of the voltage-dependent calcium channel. *Neuron* **7**, 35-44.

Klingauf, J. and Neher, E. (1997). Modeling buffered Ca2+ diffusion near the membrane: implications for secretion in neuroendocrine cells. *Biophys. J.* **72**, 674-690.

Lazarides, E. (1976). Actin, alpha-actinin, and tropomyosin interaction in the structural organization of actin filaments in nonmuscle cells. *J. Cell Biol.* **68**, 202-219.

Lopez, I., Giner, D., Ruiz-Nuno, A., Fuentealba, J., Viniegra, S., Garcia, A. G., Davletov, B. and Gutierrez, L. M. (2007). Tight coupling of the t-SNARE and calcium channel microdomains in adrenomedullary slices and not in cultured chromaffin cells. *Cell Calcium* **41**, 547-558.

Lopez, I., Ortiz, J. A., Villanueva, J., Torres, V., Torregrosa-Hetland, C. J., Frances, M. M., Viniegra, S. and Gutierrez, L. M. (2009). Vesicle motion and fusion are altered in chromaffin cells with increased SNARE cluster dynamics. *Traffic* **10**, 172-185.

Lukyanetz, E. A. and Neher, E. (1999). Different types of calcium channels and secretion from bovine chromaffin cells. *Eur. J. Neurosci.* **11**, 2865-2873.

Monck, J. R., Robinson, I. M., Escobar, A. L., Vergara, J. L. and Fernandez, J. M. (1994). Pulsed laser imaging of rapid Ca2+ gradients in excitable cells. *Biophys. J.* **67**, 505-514.

Montero, M., Alonso, M. T., Albillos, A., Cuchillo-Ibanez, I., Olivares, R., Villalobos, C. and Alvarez, J. (2002). Effect of inositol 1,4,5-trisphosphate receptor stimulation on mitochondrial [Ca2+] and secretion in chromaffin cells. *Biochem. J.* **365**, 451-459.

Neco, P., Giner, D., Viniegra, S., Borges, R., Villarroel, A. and Gutierrez, L. M. (2004). New roles of myosin II during vesicle transport and fusion in chromaffin cells. *J. Biol. Chem.* **279**, 27450-27457.

O'Sullivan, A. J., Cheek, T. R., Moreton, R. B., Berridge, M. J. and Burgoyne, R. D. (1989). Localization and heterogeneity of agonist-induced changes in cytosolic calcium concentration in single bovine adrenal chromaffin cells from video imaging of fura-2. *EMBO J.* **8**, 401-411.

Parsons, T. D., Coorssen, J. R., Horstmann, H. and Almers, W. (1995). Docked granules, the exocytic burst, and the need for ATP hydrolysis in endocrine cells. *Neuron* **15**, 1085-1096.

Pozzan, T. and Rizzuto, R. (2000). High tide of calcium in mitochondria. *Nat. Cell Biol.* **2**, E25-E27.

Robinson, I. M., Finnegan, J. M., Monck, J. R., Wightman, R. M. and Fernandez, J. M. (1995). Colocalization of calcium entry and exocytotic release sites in adrenal chromaffin cells. *Proc. Natl. Acad. Sci. USA* **92**, 2474-2478.

Sankaranarayanan, S., Atluri, P. P. and Ryan, T. A. (2003). Actin has a molecular scaffolding, not propulsive, role in presynaptic function. *Nat. Neurosci.* **6**, 127-135.

Segura, J., Gil, A. and Soria, B. (2000). Modeling study of exocytosis in neuroendocrine cells: influence of the geometrical parameters. *Biophys. J.* **79**, 1771-1786.

Starr, T. V., Prystay, W. and Snutch, T. P. (1991). Primary structure of a calcium channel that is highly expressed in the rat cerebellum. *Proc. Natl. Acad. Sci. USA* **88**, 5621-5625.

Trifaro, J. M., Rodriguez Del, C. A. and Vitale, M. L. (1992). Dynamic changes in chromaffin cell cytoskeleton as prelude to exocytosis. *Mol. Neurobiol.* **6**, 339-358.

Trifaro, J. M., Gasman, S. and Gutierrez, L. M. (2008). Cytoskeletal control of vesicle transport and exocytosis in chromaffin cells. *Acta Physiol. (Oxf.)* **192**, 165-172.